ORNL/TM-2000/172

Engineering Technology Division

DUAL MODE INVERTER CONTROL TEST VERIFICATION

J. M. Bailey, Ph.D
J. W. McKeever, Ph.D.
M. B. Scudiere, Ph.D.
G. J. Su, Ph.D.
C. W. Ayers
C. P. White
G. W. Ott
C. L. Coomer
J. S. Lawler, Ph.D.

March 2001

Prepared by the
OAK RIDGE NATIONAL LABORATORY
Oak Ridge, Tennessee 37831
managed by
UT-BATTELLE, LLC
for the
U.S. DEPARTMENT OF ENERGY
Under contract DE-AC05-00OR22725

TABLE OF CONTENTS

LIST OF FIGURES

LIST OF TABLES

ACRONYMS

BDCM	Brushless DC Motor
CPSR	Constant Power Speed Ratios
DMIC	Dual Mode Inverter Control
DOE	Department of Energy
HEV	Hybrid-Electric Vehicle
IMP	Interior Mounted PM
PEEMRC	Power Electronics and Electric Machinery Research Center
PM	Permanent Magnet
PMSM	Permanent Magnet Synchronous Motor
PNGV	Partnership for a New Generation of Vehicle
SMP	Surface Mounted PM

ABSTRACT

Permanent Magnet Motors with either sinusoidal back emf (permanent magnet synchronous motor [PMSM]) or trapezoidal back emf (brushless dc motor [BDCM]) do not have the ability to alter the air gap flux density (field weakening). Since the back emf increases with speed, the system must be designed to operate with the voltage obtained at its highest speed. Oak Ridge National Laboratory's (ORNL) Power Electronics and Electric Machinery Research Center (PEEMRC) has developed a dual mode inverter controller (DMIC) that overcomes this disadvantage. This report summarizes the results of tests to verify its operation.

The standard PEEMRC 75 kW hard-switched inverter was modified to implement the field weakening procedure (silicon controlled rectifier enabled phase advance). A 49.5 hp motor rated at 2800 rpm was derated to a base of 400 rpm and 7.5 hp. The load developed by a Kahn Industries hydraulic dynamometer, was measured with a MCRT9-02TS Himmelstein and Company torque meter. At the base conditions a current of 212 amperes produced the 7.5 hp. Tests were run at 400, 1215, and 2424 rpm. In each run, the current was no greater than 214 amperes. The horsepower obtained in the three runs were 7.5, 9.3, and 8.12.

These results verified the basic operation of the DMIC in producing a Constant Power Speed Ratios (CPSR) of six.

1. INTRODUCTION

1.1 Background

Permanent magnet (PM) motors have excellent features which may be exploited by hybrid-electric vehicles (HEVs), but they will require development of a cost effective method for operating them at least five times higher than base speed as indicated by performance curves generated in December 1998, by the Partnership for a New Generation of Vehicles (PNGV). The base speed is the highest speed at which the rated torque is developed and is a function of the inverter's supply voltage.

This very important speed range above base speed is considered by the PNGV to be the speed range over which rated power can be generated; however, the typical PM motor/inverter system does not operate well above base speed. Unless the magnet field is "weakened" physically or unless current is injected during low voltage portions of the back-emf waveform by inverter control, the PM motor will have to be designed so that the back-emf doesn't reach the required bus voltage before it reaches its maximum operating speed. The penalty for such over-design is that the inverter voltage and current ratings must be appropriately increased. This type of penalty is likely to cause unjustified and premature disqualification of PM motor/drive system technology.

PM motors can be classified as to the shape of their back-emf. PM motors with trapezoidal back-emf are termed brushless dc motor (BDCM) and those with sinusoidal back-emf are termed PM synchronous motor (PMSM). These motors can be further classified by the way the PMs are fastened to the rotor. PMs for surface mounted PM (SMP) motors are attached to the periphery. PMs for interior mounted PM (IMP) motors are buried in the interior of the rotor. PMSMs can have either SMPs or IMPs. BDCMs have SMPs.

In FY 1998, the Power Electronics and Electric Machinery Research Center (PEEMRC) began a Department of Energy (DOE) sponsored investigation to see if known field-weakening methods could be generalized and applied to a PM traction motor (BDCM or PMSM) with surface mounted magnets and whether there are problem areas that might limit the utilization of these techniques [1].

A review of known methods for efficiently controlling the inverter for PMSM motors found that the voltage and current must fall inside an area intersected by a voltage ellipse and a current circle. It has been shown that PMSMs with surface mounted magnets can be successfully operated at constant power speed ratios (CPSRs) of 3 or 4. One PM motor with interior mounted magnets achieved a CPSR of 7.5; however, most available commercial PM motors have surface mounted magnets because they are easier to manufacture.

It was found that the performance of PMSMs and BDCMs with surface mounted magnets was highly dependent upon the motor inductance. An equation was developed for the maximum CPSR for a given power and inductance. It indicated that the necessary inductance value could be reduced by designing the PM to have a lower back-emf, more magnetic poles, a higher base

speed, and higher current. One intriguing solution was the phase advance method [2]. It is effective in controlling the motor power over such a speed range but the current at high speed may be several times greater than that required at the base speed. The increase in current during high-speed operation is due to the low motor inductance and the action of the bypass diodes of the inverter. The use of such a control would require increased current rating of the inverter semiconductors and additional cooling for the inverter, where the conduction losses increase proportionally with current, and especially for the motor, where the copper losses increase with the square of the current. The high current problems of phase advance can be mitigated by adding series inductance [3]; however, this reduces power density, requires a significant increase in supply voltage, and leaves the CPSR performance of the system highly sensitive to variations in the available voltage.

A new dual mode inverter control (DMIC) that overcomes these drawbacks has been developed, built, and tested. This report documents these results.

1.2 DMIC Operation [4]

Figure 1.1 shows the complete system as it would be utilized in the HEV application. Figure 1.2 is the common voltage-fed inverter used with the phase advance method of Ref. 2 and Fig. 1.3 the DMIC.

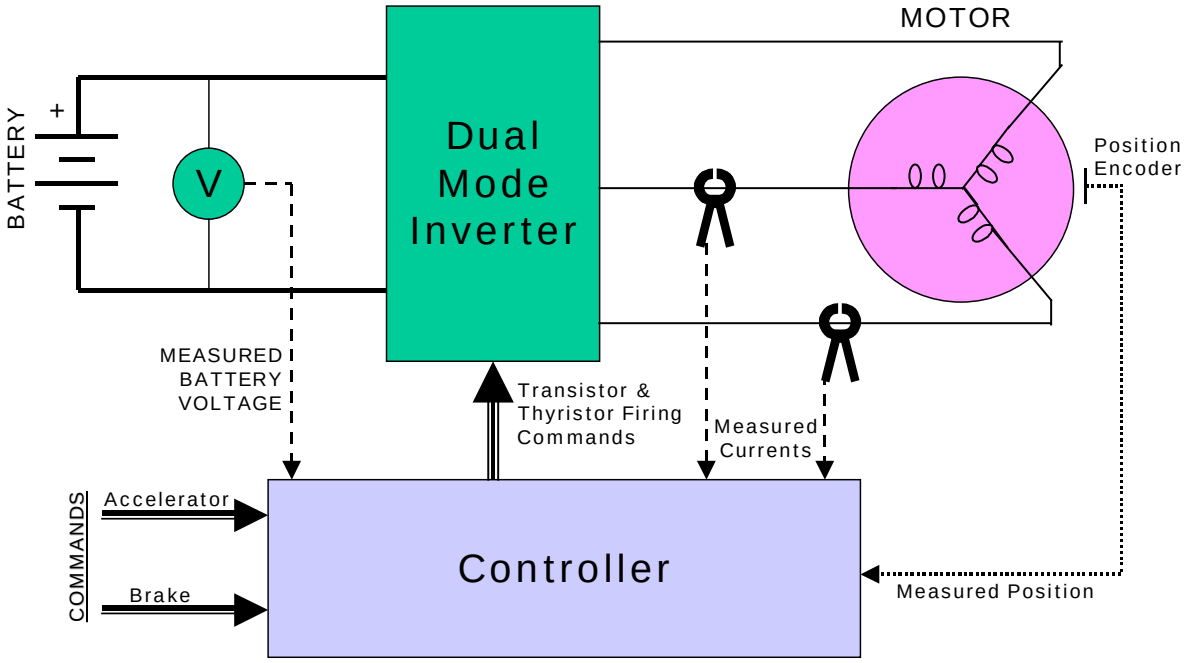

Fig. 1.1. DMIC test system block diagram.

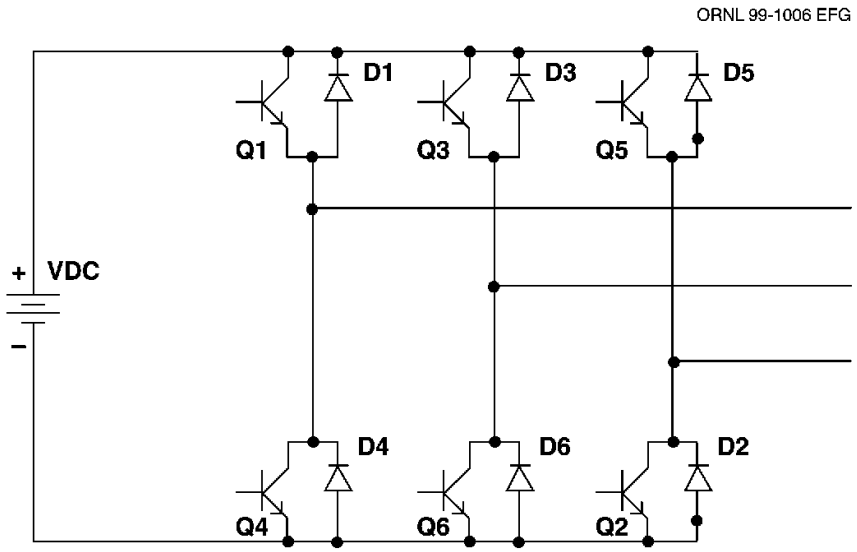

Fig. 1.2. Common voltage-fed inverter topology used with phase advance.

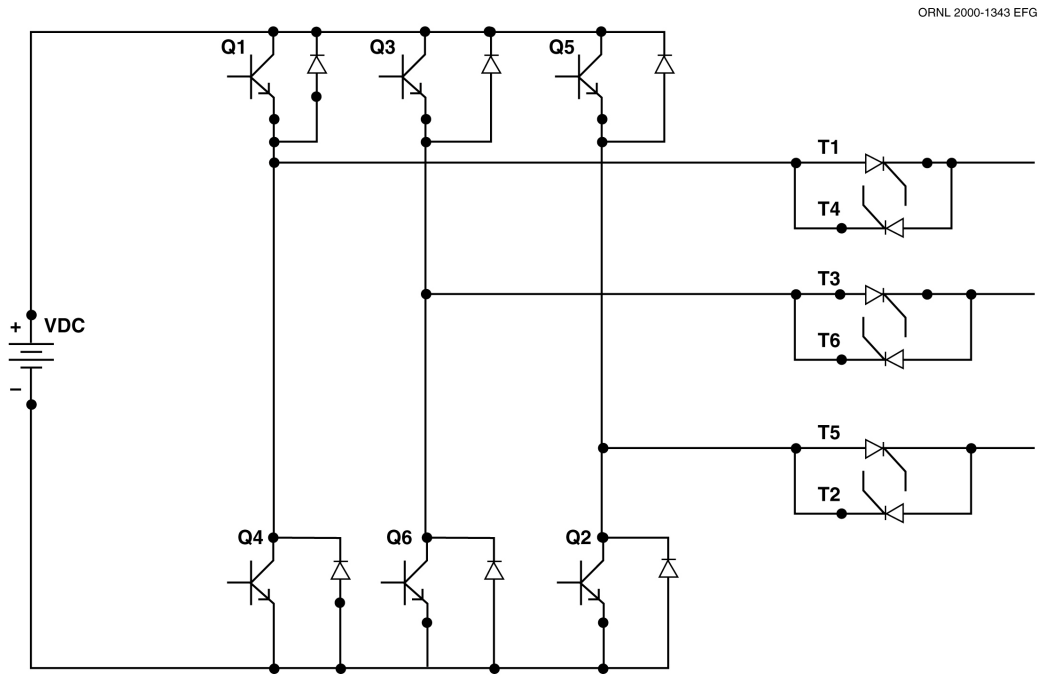

Fig. 1.3. Dual mode inverter topology.

In the DMIC, the conventional inverter output is interfaced to the motor through a thyristor-based ac voltage controller as shown in Fig. 1.3. If in a given phase the two transistors are off, phase current can flow through one of the bypass diodes provided one of the thyristors in that phase is on. This current however will not be allowed to reverse. Once the phase current reaches zero, the conducting thyristor shuts off and no matter what the internal potential of that phase may be the phase is isolated from the supply until such time as one of the transistors, and a

companion thyristor are fired. This scheme allows commutation to occur, but once the outgoing phase current reaches zero there is no further conduction until the next time that the phase is intentionally fired. Thus, each pole of the DMIC inverter has three states; a given phase can be connected to the positive rail of the supply, connected to the negative rail of the supply, or isolated from the supply when all transistors and thyristors in that phase are off.

Below base speed, the DMIC uses the normal BDCM control scheme and operates on two phases at a time, except for the short commutation intervals when all three phases are conducting. The ability of the DMIC inverter to isolate one phase from the supply allows the single-phase operation concept (current passes through only two phases at a time) to be extended to high-speed operation. The term dual mode applies to the fact that below base speed, power regulation is achieved by modulating the conduction of the transistors and involves high frequency switching. The switching rate depends on the hysteresis band within which phase current is allowed to vary around its desired value. Above base speed all of the transistors are switched at the fundamental rate.

While the transistors are modulated for regulation below base speed, which may involve PWM kilohertz switching rates, the thyristors do not participate in the regulation and are always fired at the fundamental rate as determined by motor speed. Above base speed, all of the devices are fired at the fundamental rate.

In the DMIC inverter, once a fault is detected, thyristor firing can be inhibited to prevent the motor from feeding the fault despite the fact that the rotor continues to spin. The motor fault current would be extinguished within one sixth of a fundamental cycle after the fault is detected and further thyristor firing is disabled.

The firing scheme of the DMIC controller for the motoring mode of operation is shown in Fig. 1.4. The transistors are fired at an advance angle, θ_a, but the advance angle is defined relative to the intersection of one of the phase-to-phase back-emfs with the dc supply voltage. Figure 1.4 shows the firing scheme for the transistors and thyristors of phase a referred to the line-to-line emf e_{ab}. The firing of the semiconductors in phase b would be completely analogous to Fig. 1.4 with the relevant line-to-line emf being e_{bc} and the firing in phase c would be referred to the voltage e_{ca}. There are six distinct intervals which involve one phase being connected to the positive rail of the dc supply and one phase being connected to the negative rail of the supply. Each interval lasts for 60 electrical degrees before one of the conducting phases is exchanged for the idling phase. Once a phase is energized it remains energized for two 60 degree intervals before being rotated out as the idling phase. Firing before the intersection of e_{ab} with V_{dc} allows current to be driven into the phase a winding since V_{dc} is greater than eab at the time that Q1 and T1 are fired.

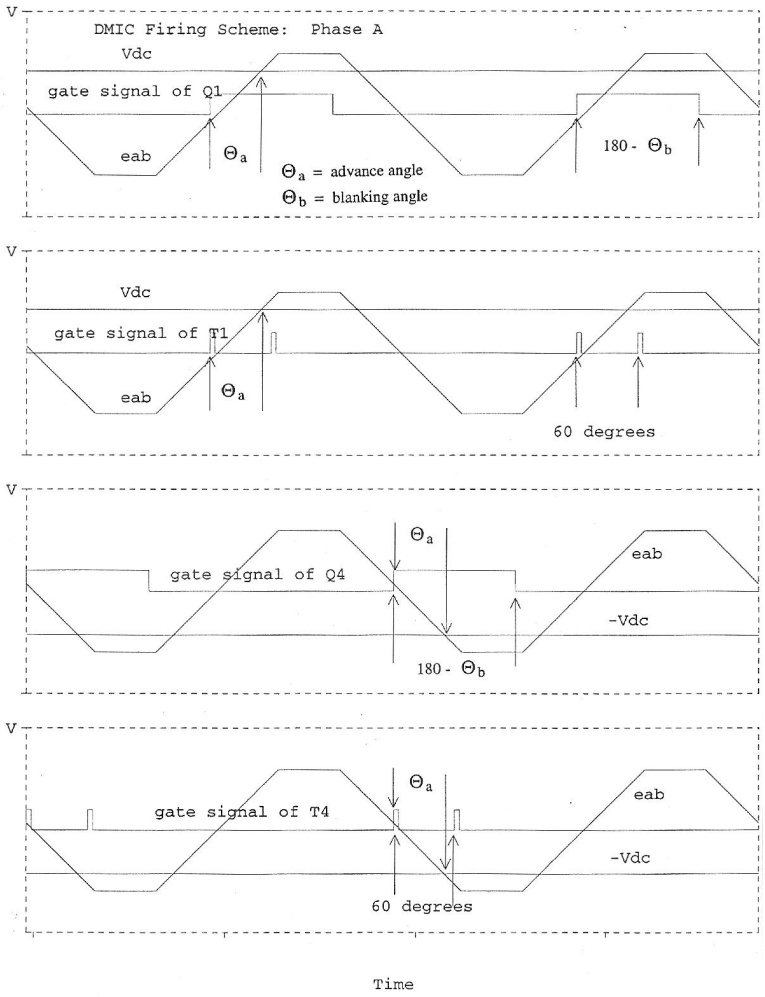

Fig. 1.4. Firing scheme of the DMIC in the motoring mode, Phase A.

Each odd (even) numbered thyristor is fired at the same time as the corresponding odd (even) numbered transistor and is fired again 60 degrees later. The second firing is necessary at low advance angles where the incoming phase current rises but falls to zero before the end of the first 60 degree interval due to the back-emf exceeding V_{dc}, and when the current reaches zero the thyristor shuts off. If the phase current during the first 60 degree interval falls to zero then the thyristor must be re-triggered at the start of the second interval. When the phase advance is large, the phase current will not be zero at the end of the first 60 degree interval and the thyristor will remain on and not need to be re-triggered. In such cases, the second firing pulse is redundant but doesn't do any harm.

The commanded conduction angle in the DMIC can vary from 120 and approach 180 degrees. In Fig. 1.4, the transistor conduction angle is denoted as 180 degrees minus θ_b which is the "blanking angle." In a PWM inverter, some time is set aside between the time that one transistor in a given phase pole is to be turned off and before the opposite transistor in that pole is to be turned on. This is referred to as the blanking time and it is a safeguard against inadvertent short circuits of the supply due to variations in the turn off and turn on times of the transistors. There is no worry over inadvertent short circuits of the supply in the DMIC. However, there is good

reason to run the blanking angle from 60 degrees towards 0 degrees. At a commutation time, the phase current in the outgoing phase may be large, but decreasing in magnitude due to the emf crossing Vdc, and that phase is contributing a great deal of power (simultaneously high current and high voltage). At a blanking angle of 60 degrees, the outgoing phase is shut off by turning off the appropriate transistor and allowing the phase current to transfer to the bypass diode of the opposite transistor. Recall that the thyristor supporting this phase current shuts off when the current reaches zero. This sudden reversal of the outgoing phase from one rail of the supply to the opposite rail hastens commutation of the outgoing phase to off; however, since the outgoing phase current is already decreasing allowing the outgoing transistor to stay on longer will slow down the commutation process. Slowing down commutation prolongs the period of simultaneous high current-high voltage in the outgoing phase. So long as the current in the outgoing phase reaches zero within the allowable 60-degree interval the amount of power developed will be increased, and substantially so, at the expense of a slight increase in rms current.

The transition from below base speed operation to above base speed is a mixture of phase advance, involving adjustment of the advance angle, θ_a, and the blanking angle, θ_b, as well as the set-point of the phase current regulator. Smooth adjustment by the transition control is important in electric vehicle applications so that the operator experiences smooth changes in vehicle speed in the vicinity of the base speed of the motor. The details of the transition control will be reported in subsequent work.

1.3 Report Outline

In Chapter 2, the elements and instrumentation of the test will be detailed. Chapter 3 will then show the test results and how they serve as proof of the DMIC's ability to perform its tasks.

2. TEST ELEMENTS

2.1 Introduction

For the test phase the system of Fig. 1.1 was emulated by that of Fig. 2.1. Here, the "battery" was an Electronic Measurements, Inc. dc power supply. The diodes D-7 provided protection for reverse current surges. The dual mode inverter consists of the ORNL 75 kw hard-switched inverter with the SCR's attached as a separate unit. The electric motor is one developed by ORNL and is discussed in Section 2.2. The controller consists of the ORNL Universal Motor Controller Interface unit and a TMS 320C40 DSP controller card. The card, along with the appropriate algorithms, is embedded in a personal computer.

The load is developed by a Kahn Industries, Inc. hydraulic dynamometer and is discussed in Section 2.3. The test director commands the desired speed and the dynamometer is adjusted to obtain the desired torque and hence horsepower. This procedure requires several adjustments between the test director and the water brake operator.

2.2 The Electric Motor

The test motor is an axial gap PM brushless dc motor (BDCM). The back emf wave shape is trapezoidal as shown in Fig. 2.2 where n is the multiple of base speed.

The equivelant and circuit is shown in Fig. 2.3 with the measured parameters of

N_b = base speed = 2600 rpm
L_s = 61.8μH
M = 11.8μH
R = 0.0118 ohms (2.1)
E_b = peak phase-to-neutral back emf at base speed = 74.2 volts
P_r = rated power = 36,927 watts (49.5 horsepower)
V_{ab} = dc supply voltage = 162 volts

The 162 volt supply is the voltage required by the motor. Any voltage drop in the inverter would increase the inverter supply voltage requirement.

For the classical idealized rectangular phase current wave shape of the BDCM (rectangular shape of 120 degrees duration each half cycle), the theoretical peak and rms currents of this motor are:

$$I_{pk} = \text{peak current} = \frac{P_r}{2E_b} = 249 \text{ amps}$$

$$I_{rms} = \text{rms current} = I_{pk}\sqrt{\frac{2}{3}} = 203.3 \text{ amps} \quad (2.2)$$

Although the referenced specifications of Section 1.1 require a CPSR of 5:1, it was decided to design the test for a CPSR of 6:1 to emphasize the DMIC's utility. However, the motor was designed for a maximum speed of 2800 rpm. Thus, it was decided to choose 400 rpm as the base speed so that a measurement could be safely taken at 2400 rpm.

Derating the motor horsepower by the ratio of the chosen base speed of 400 rpm to that of its rated speed of 2600 rpm would lead to a value of 7.6 hp. Thus, the simulation shown in Fig. 2.4 was performed that indicated 7.48 hp as the base horsepower. The motor was then connected to the dynamometer and brought to a speed of 400 rpm. The dc supply voltage was gradually increased until 7.5 hp was obtained at 41.9 volts. This voltage was then used in the tests discussed in Chapter 3.

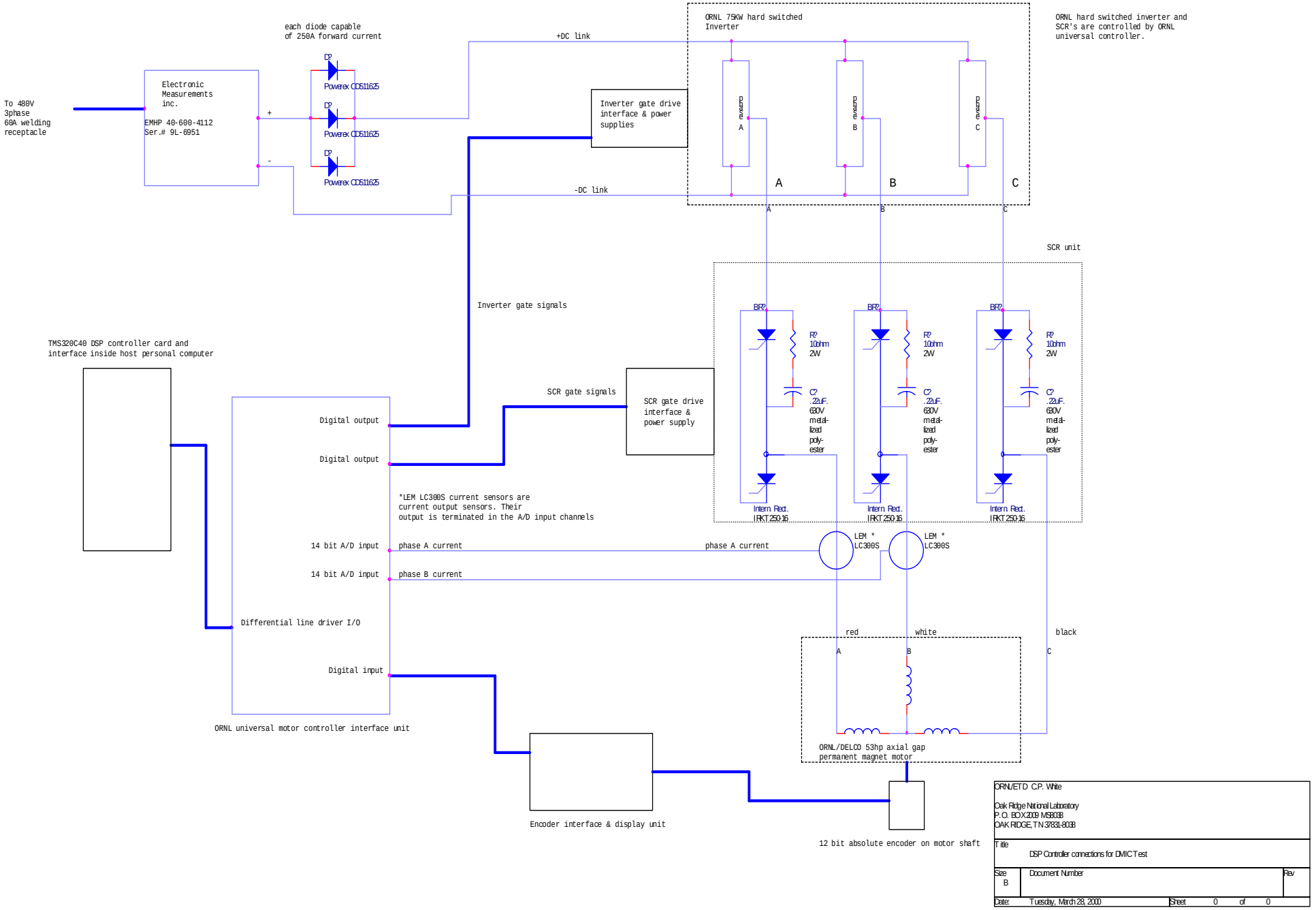

Fig. 2.1. Test elements.

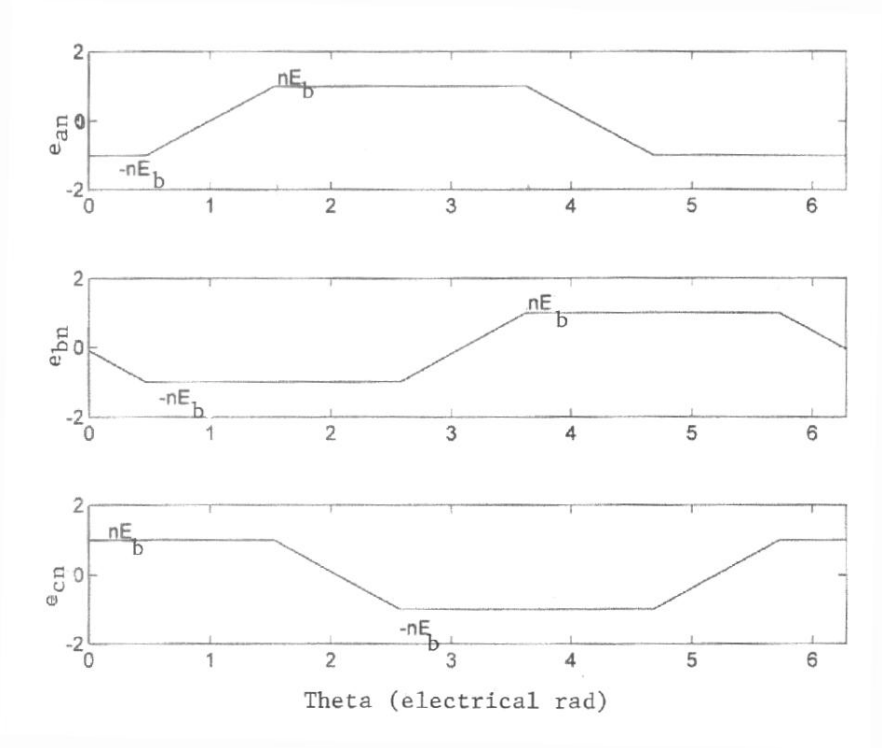

Fig. 2.2. Back-emf waveshapes of the BDCM.

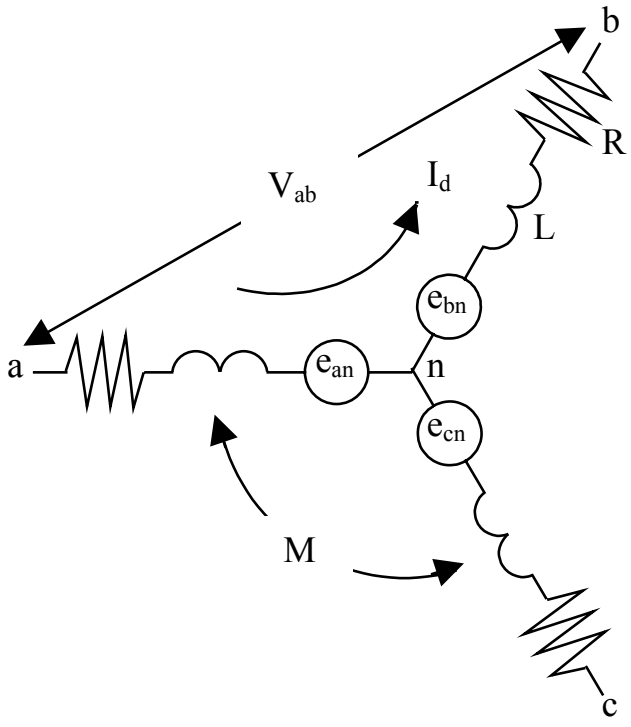

Fig. 2.3. Motor equivelant circuit.

2.3 Water Brake

The water brake is a hydraulic dynamometer model 101-080 manufactured by Kahn Industries. Hydraulic dynamometers convert mechanical energy into heat. Water is utilized to provide resistance to rotation and to remove the heat. The relationship for water flow, temperature, and horsepower is

$$Q = \frac{5.09\ P}{t_2 - t_1}, \tag{2.3}$$

where

Q = flow rate gal/min,
P = adsorbed power hp,
t_1 = inlet temperature °F, and
t_2 = outlet temperature °F.

The developed torque is measured by a model MCRT9-02TS Himmelstein and Company torque meter with a maximum rating of 6000 lb-inch and 7500 rpm. A picture of the water brake is shown in Fig. 2.5 and the absorption curve in Fig. 2.6. A more general description is included in Appendix A.

The motor torque meter and brake are connected as shown in Fig. 2.7. To obtain 7.5 hp at 400 rpm it was necessary to add the disk brake to the water brake. A sketch of the disk brake is shown in Fig. 2.8. The disk brake is mounted on the shaft of the water brake. With the tooth ratio T as shown in Fig. 2.7,

$$T = \frac{T_1}{T_2} = \frac{112}{34} = 3.294\,. \tag{2.4}$$

The map of motor speed and water brake speed becomes that of Table. 2.1.

Table 2.1. Motor speed vs water brake speed

Motor Speed RPM	Water Brake Speed RPM
400	1317.6
1000	3294
1500	4941
2000	6588
2400	7905.6

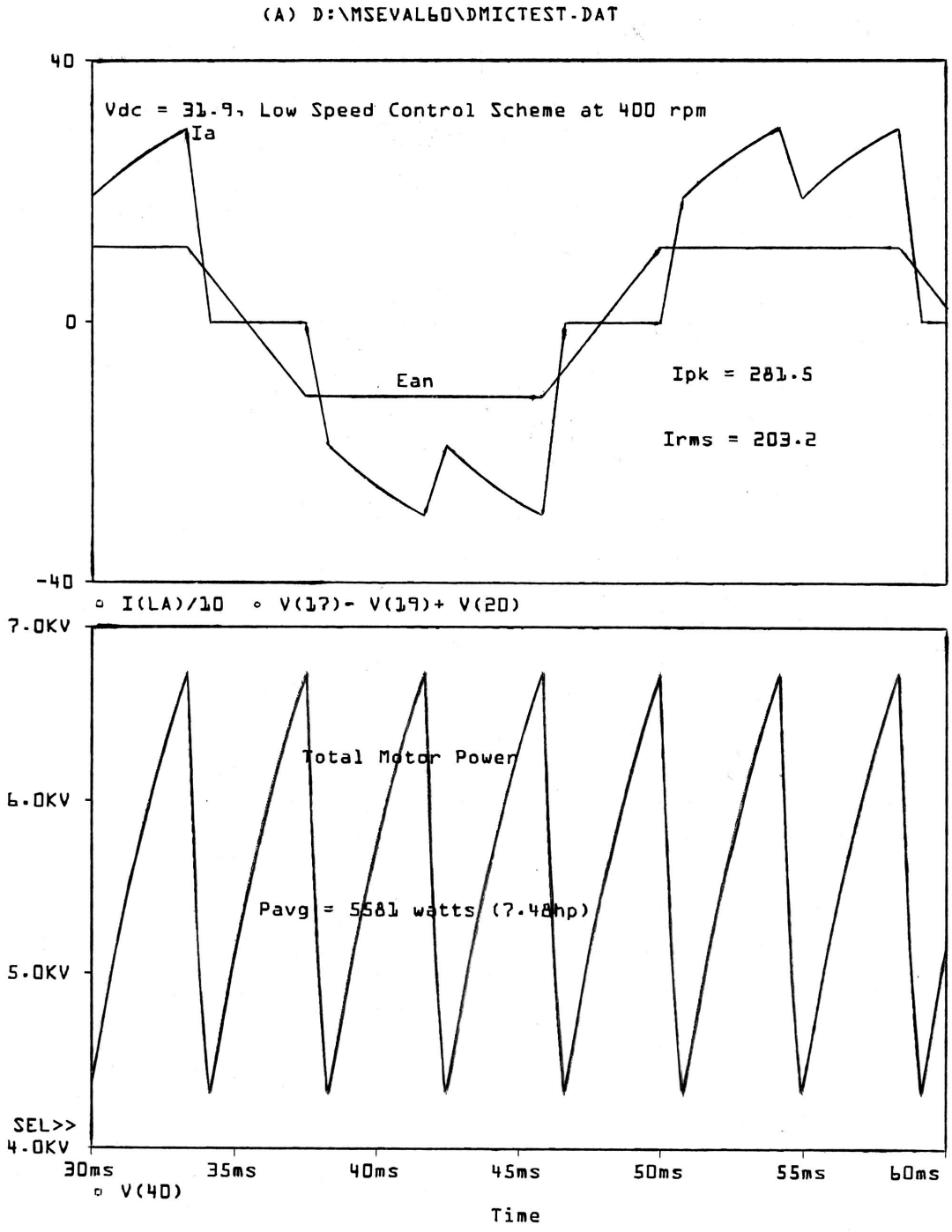

Fig. 2.4. Choosing base horsepower.

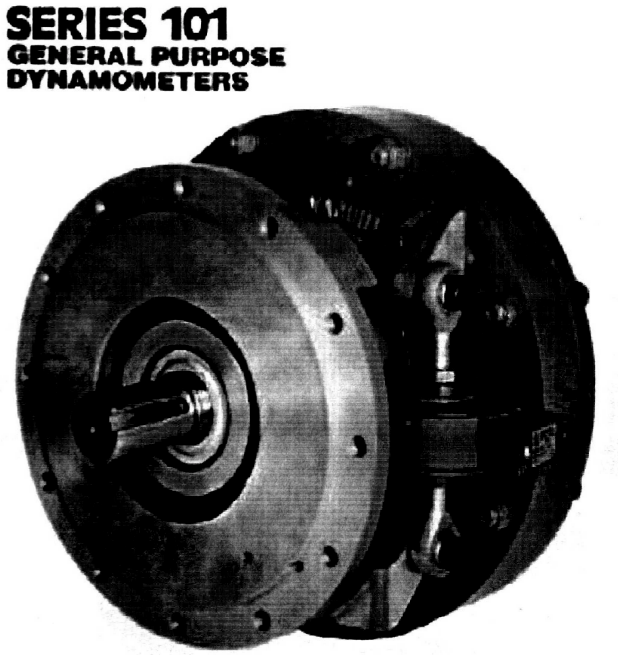

Fig. 2.5. Kahn water brake power absorber.

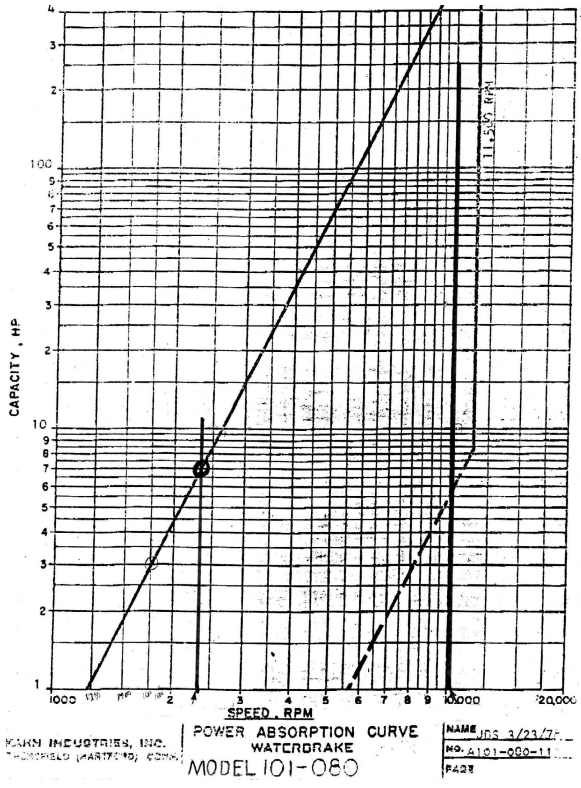

Fig. 2.6. Water brake power absorption curve for Kahn Model 101-080.

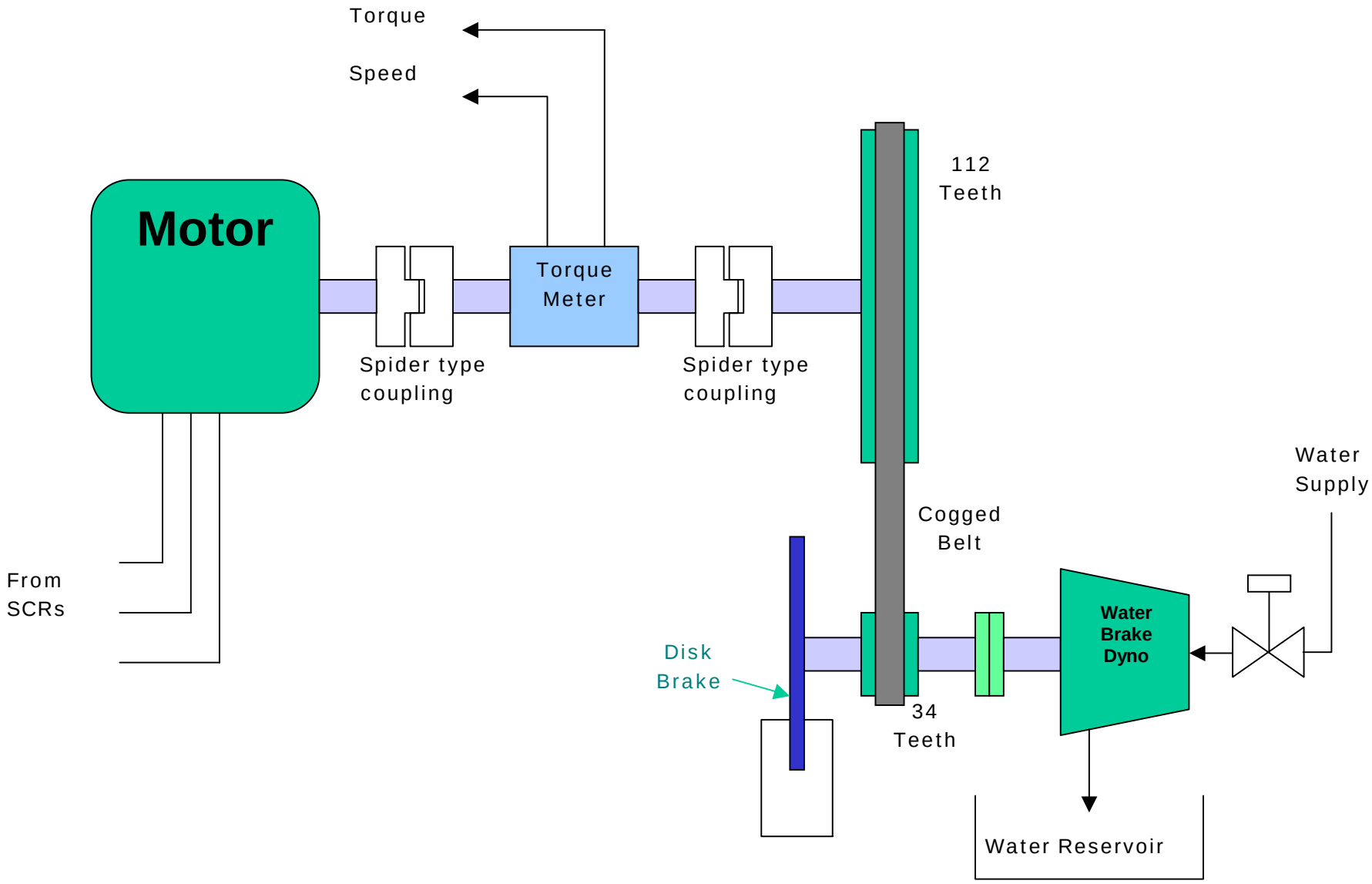

Fig. 2.7. Motor/torque meter/water brake interfaces.

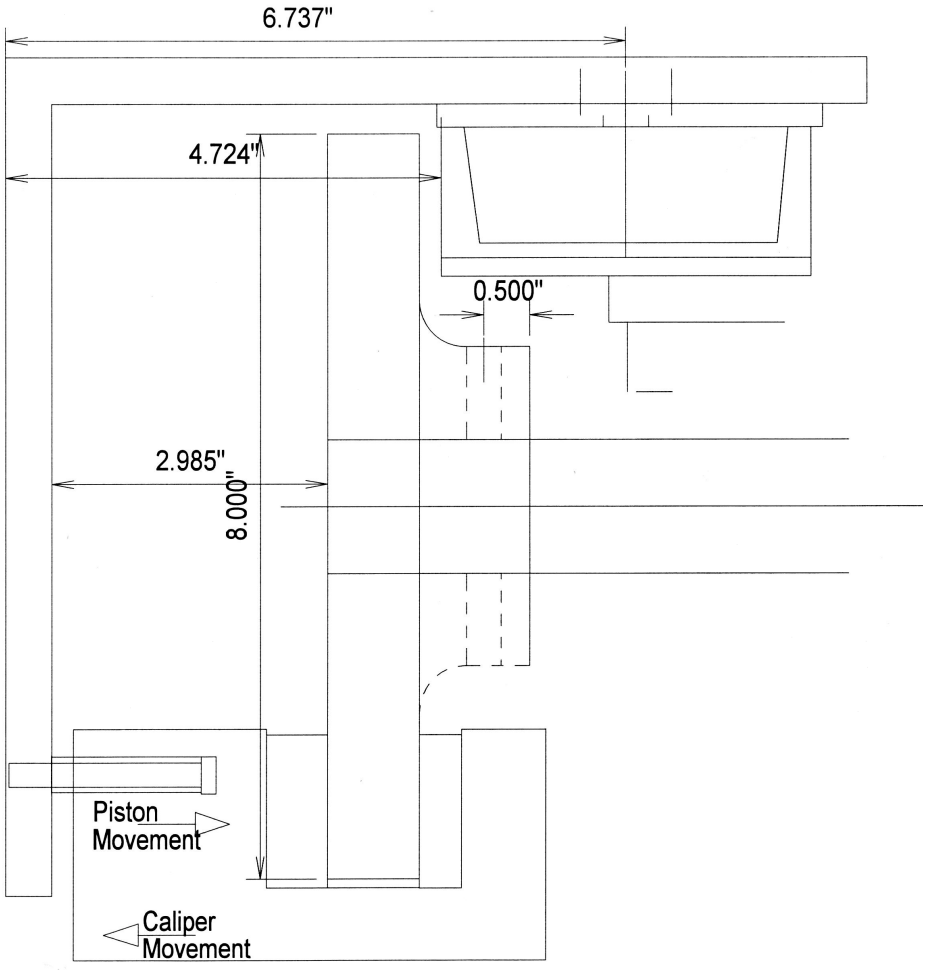

Fig. 2.8. Disk brake for power measurement at low rpm.

2.4 Instrumentation

The instrumentation system is shown in Fig. 2.9. The heart of the system consists of two Yokogawa power meters, a model WT2030 measuring current, voltage, and power between the inverter and the SCRs, and a model PZ4000 measuring the same quantities between the SCRs and the test motor. The PZ4000 was also configured to read the dc link current and voltage and hence the input power to the system. A Yokokawa DL7100 oscilloscope with a Tektronic A6909 isolator was used to monitor the a-phase voltage waveform referenced to the negative dc link for comparison with a computer simulated waveform. The DL7100 also monitored the cycle initiating pulse, its phase relation to the transistor (IGBT) and thyristor (SCR) gate signals, and the resulting current in phase a.

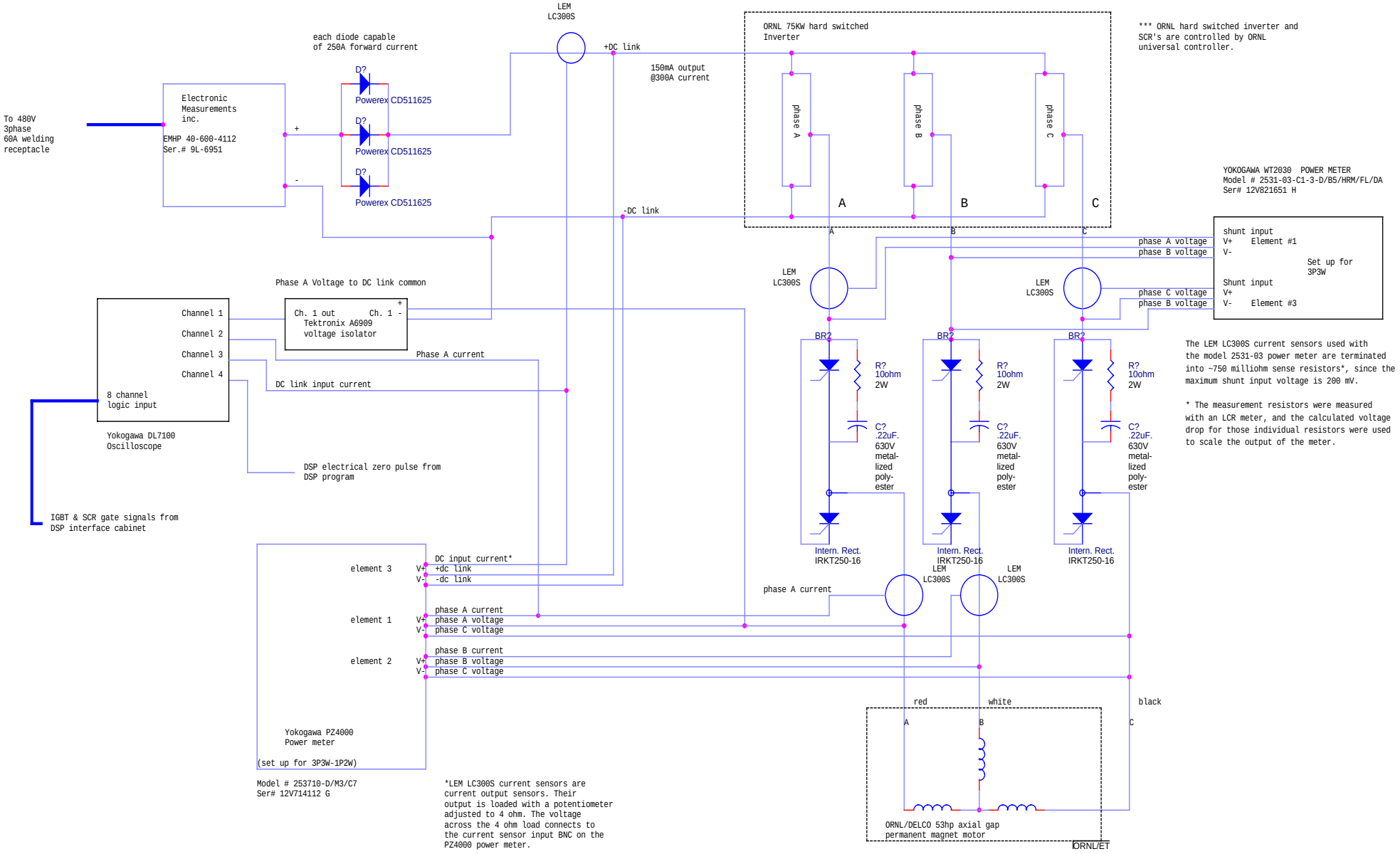

Fig. 2.9. Test instrumentation.

The Yokogawa PZ4000 power meter can perform the functions shown in Table 2.2. Its output appears in the form shown in Fig. 2.10. The data is presented in six columns titled Element 1, Element 2, Element 3, Element 4, ΣA, and ΣB. The power is measured by the two-watt meter method using V_{ac}, I_a, V_{bc}, and I_b. The data, circled in Fig. 2.10, is apportioned among the six columns as shown in Table 2.3. The accompanying plot may show any of the measured variables, which in this example is I_A. The WT2030 Yokogawa power meter does not have this capability, but presents its data in the tabular form of Fig. 2.11. Since it too uses the two wattmeter method one set of the voltage and currents are zero. The phase power, 8.18 kW, (now row 12) is the sum of rows 3 and 9.

Table 2.2. Symbols and determination of measurement functions (5)

Measurement Functions in the Normal Measurement Mode

Measurement Functions in the Normal Measurement Mode		Determination, Equation					
U [V]	Urms Umn Udc Uac U+pk U-pk	Urms	Umn	Udc	Uac	U+pk	U-pk
		$\sqrt{\frac{1}{T}\int_0^T u(t)^2\,dt}$	$\frac{\pi}{2\sqrt{2}}\frac{1}{T}\int_0^T \lvert u(t)\rvert\,dt$	$\frac{1}{T}\int_0^T u(t)\,dt$	$\sqrt{Urms^2 - Udc^2}$	Maximum	Minimum
I [A]	Irms Imn Idc Iac I+pk I-pk	Irms	Imn	Idc	Iac	I+pk	I-pk
		$\sqrt{\frac{1}{T}\int_0^T i(t)^2\,dt}$	$\frac{\pi}{2\sqrt{2}}\frac{1}{T}\int_0^T \lvert i(t)\rvert\,dt$	$\frac{1}{T}\int_0^T i(t)\,dt$	$\sqrt{Irms^2 - Idc^2}$	Maximum	Minimum
fU, fI [Hz]		The voltage frequency (fU) and current frequency (fI) are measured using zero crossing detection.					
FfU, FfI		Voltage form factor $FfU = \frac{Urms}{\frac{2\sqrt{2}}{\pi}Umn}$			Current form factor $FfI = \frac{Irms}{\frac{2\sqrt{2}}{\pi}Imn}$		
CfU, CfI		Voltage crest factor $CfU = \frac{Upk}{Urms}$ Upk = IU+pkI or IU-pkI which ever is larger			Current crest factor $CfI = \frac{Ipk}{Irms}$ Ipk = II+pkI or II-pkI which ever is larger		
P [W]		$\frac{1}{T}\int_0^T u(t)\cdot i(t)\,dt$					
S [VA]		Urms · Irms (Umn · Imn) (Udc · Idc) Can combine rms, mn, and dc. See section 10.4.					
Q [var]		$\sqrt{S^2 - P^2}$					
λ		$\frac{P}{S}$					
ϕ [°]		$\cos^{-1}\left(\frac{P}{S}\right)$ The display format of the phase difference can be switched between Lead/Lag format and 360° format. See section 10.6.					
Z [Ω]		$\frac{Urms}{Irms}$					
Rs [Ω]		$\frac{P}{Irms^2}$					
Xs [Ω]		$\frac{Q}{Irms^2}$					
Rp [Ω] (=1/B)		$\frac{Urms^2}{P}$					
Xp [Ω] (=1/G)		$\frac{Urms^2}{Q}$					
Pc [W]		IEC76-1(1976), IEEE C57.12.90-1993			IEC76-1(1993)		
		$\frac{P}{P1 + P2\left(\frac{Urms}{Umn}\right)^2}$ P1, P2 : Coefficients as defined in the applicable standard			$P\left(1 + \frac{Umn - Urms}{Umn}\right)$		

Note

- The period T is determined by the measurement/computation period setting. t = 0 is the start point and t = T is the end point. For details, see section 10.1.
- u(t) and i(t) denote the sampled data of the voltage signal and the current signal, respectively.

YOKOGAWA ♦ Uover:■ ■ ■ ■ 1s 100kS/s

∿CH1 300Vpk Iover:■ ■ ■ ■ 1s 100kS/s

	Element1	Element2	Element3	Element4	Σ A	Σ B
Urms[V]	25.91	25.98	41.90	0.0000k	25.94	41.90
Umn [V]	25.37	25.46	46.50	0.0000k	25.42	46.50
Udc [V]	0.02	0.01	41.87	0.0000k	0.02	41.87
Uac [V]	25.91	25.98	1.62	0.0000k	25.94	1.62
Irms[A]	0.2113k	0.2129k	0.2456k	0.000	0.2121k	0.2456k
Imn [A]	0.1955k	0.1966k	0.2594k	0.000	0.1961k	0.2594k
Idc [A]	-0.0000k	0.0001k	0.2335k	0.000	0.0000k	0.2335k
Iac [A]	0.2113k	0.2129k	0.0761k	0.000	0.2121k	0.0761k
P [W]	3.73k	3.86k	9.74k	-0.000k	7.59k	9.74k
S [VA]	5.47k	5.53k	10.29k	0.000k	9.53k	10.29k
Q [var]	4.01k	3.96k	3.32k	0.000k	7.97k	3.32k
λ [ ]	0.6816	0.6974	0.9464	Error	0.7962	0.9464

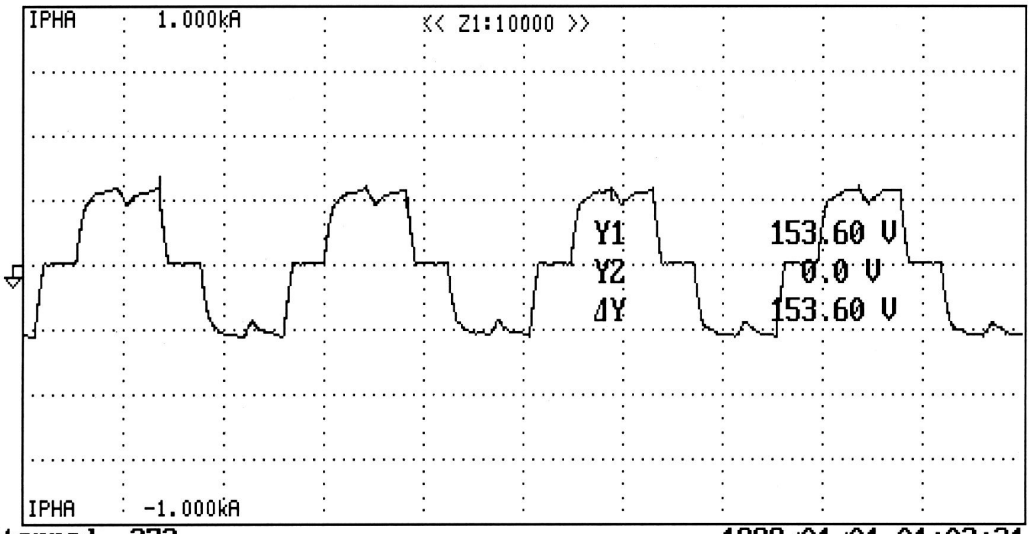

Stopped 273 1999/01/01 01:02:31

Fig. 2.10. Output of Yokogowa PZ4000 power meter.

Table 2.3 Data format

ROW	DATA
Element 1	I_A and V_{ac}
Element 2	I_B and V_{bc}
Element 3	DC link current and voltage
Element 4	Not used
ΣA	3ϕ power to motor
ΣB	Input power to inverter

The data from the PZ4000 power meter is stored in ASC11 and TIFF files. The disk number, file name, and time sensitivity of the plots are shown in Appendix B.

Figure 2.12 shows the output of the DL7100 oscilloscope. The 12 waveforms in this figure from top to bottom are listed in Table 2.4.

Normal Manual			2000.02.01 17:50:32
V	1	27.96	Vrms
A	1	206.7	Arms
W	1	4.16	kW
V	2	0.0	Vrms
A	2	0.000	Arms
W	2	0.000	kW
V	3	27.94	Vrms
A	3	205.7	Arms
W	3	4.03	kW
V	Σ	27.95	Vrms
A	Σ	206.2	Arms
W	Σ	8.18	kW
HzV	1	122.187	Hz

Fig. 2.11. Output of Yokogawa WT2030 power meter showing power between inverter and SCR5.

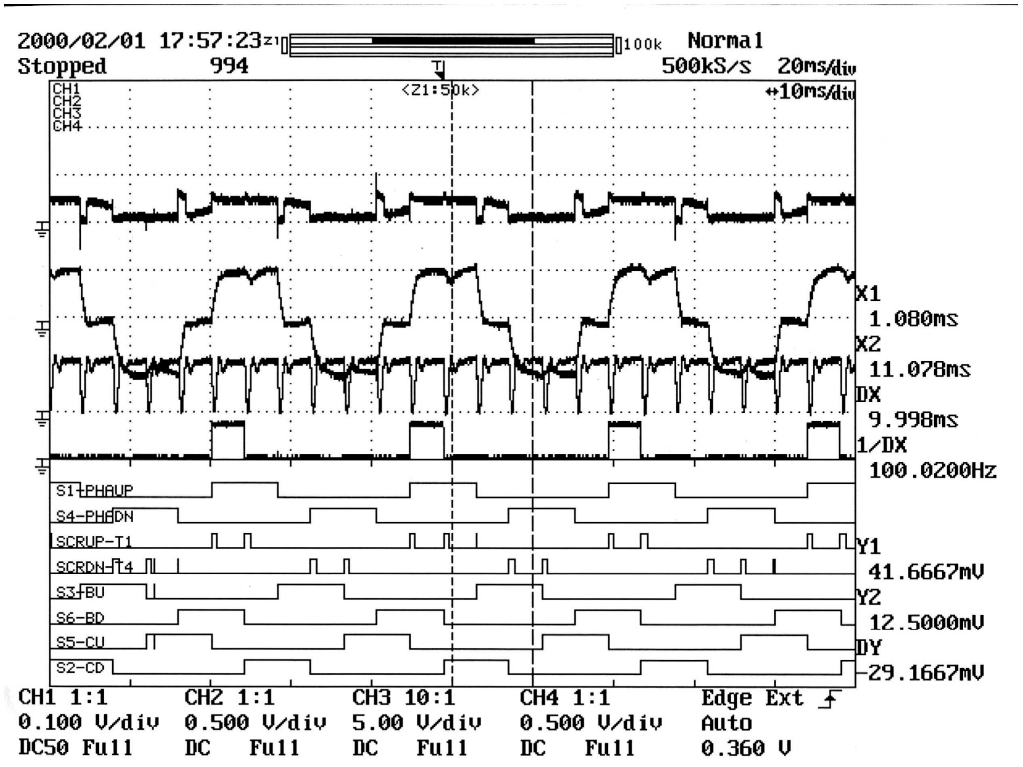

Fig. 2.12. Output of the DL7100 oscilloscope (disk 6, run 4, file FwdLoo2.TIF).
Table 2.4. DL7100 oscilloscope data format

ROW	DATA	SENSITIVITY
1	Phase A Voltage to Dc Link Common	100V/Division
2	Phase A Current	250A/Division
3	DC Link Current	250A/Division
4	Electrical 0 Pulse from Program	
5	Q1 Phase a Up Signal	
6	Q4 Phase A Down Signal	
7	T1 Up Signal	
8	T4 Down Signal	
9	Q3 Phase B Up	
10	Q6 Phase B Down	
11	Q5 Phase C Up	
12	Q2 Phase C Down	

3. TEST RESULTS

3.1 Introduction

As explained in the preceding sections, the controller of Fig. 1.1 has not been developed and its function is performed by the interplay of the test director and water brake operator. It was decided to verify the DMIC's ability by establishing two "verification boundaries," one a torque boundary and the other a current boundary.

The system was first adjusted to produce 7.5 hp at the base speed of 400 rpm. The battery voltage was set at 41.9 volts. The current at these conditions was 212 rms amperes. Thus, the horsepower and current boundaries were established. As the speed was incrementally increased, the torque was adjusted to maintain the 212 amp boundary. In all cases, the horsepower was maintained at least at 7.5 hp. This procedure was continued until a CSPR of six was obtained.

The results are now discussed.

3.2 Tests Results

While many runs were made during these tests, the six runs shown in Table 3.1 constitute the DMIC's verification performance; the output data from the DL7100 power meter is shown in Figs. 3.1–3.6. Runs 1, 2, and 4 are stored in Disk 6 as TIFF files. Runs 3, 5, and 6 were not stored on disk.

Table 3.1. DMIC test data

Run Number	Link Voltage	Speed RPM	hp	Motor RMS Current
1	43.7	2040	7.5	170
2	40.0	2010	7.55	203
3	40.0	1026	7.42	174
4	41.9	400	7.5	212
5	41.9	1215	9.27	214
6	41.9	2424	8.12	206

The results of the runs 2–6, shown in Table 3.1, are presented in graphical form in Fig. 3.7 and 3.8.

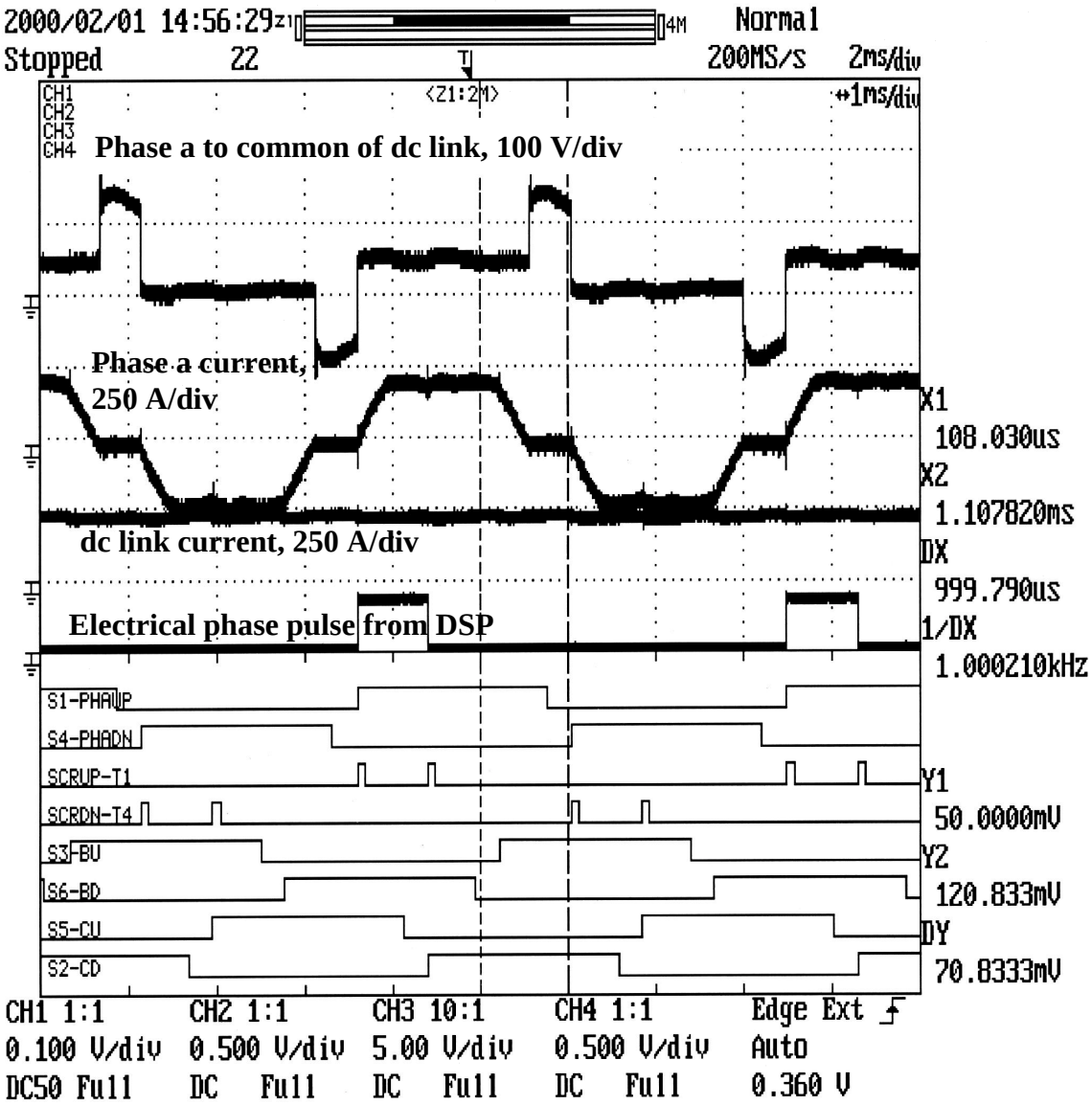

Fig. 3.1. Run 1.

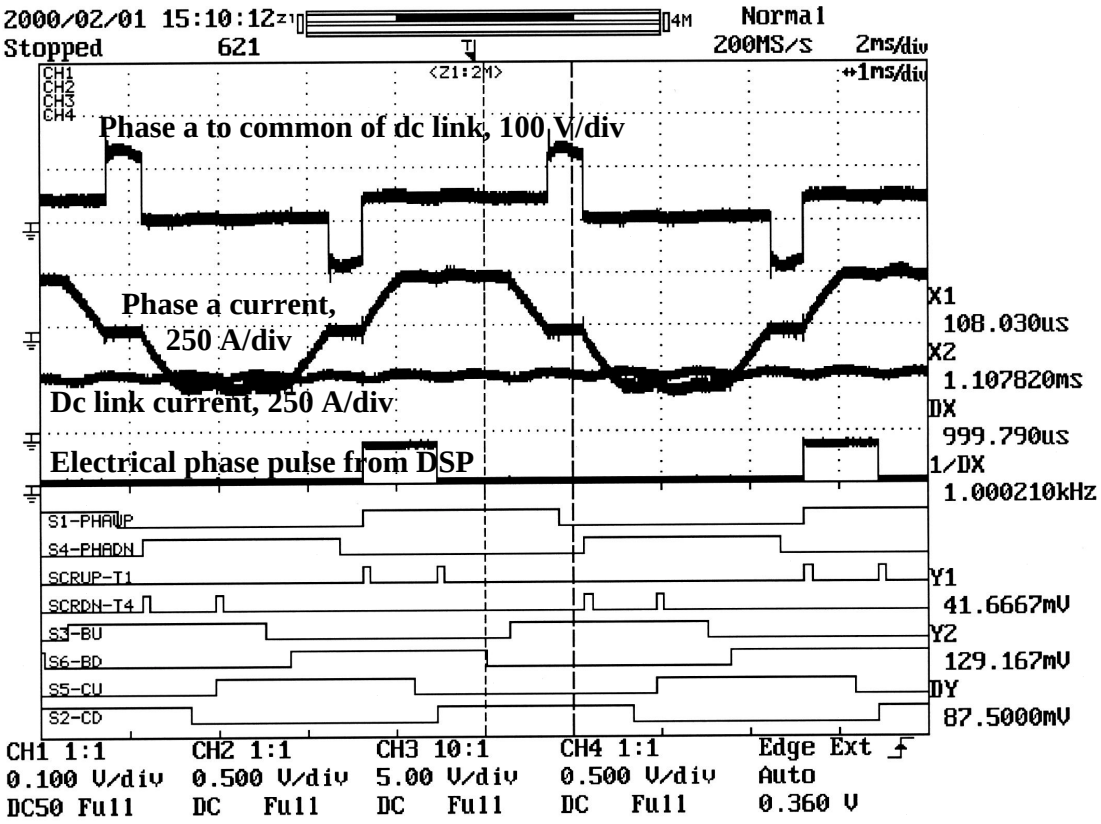

Fig. 3.2. Run 2.

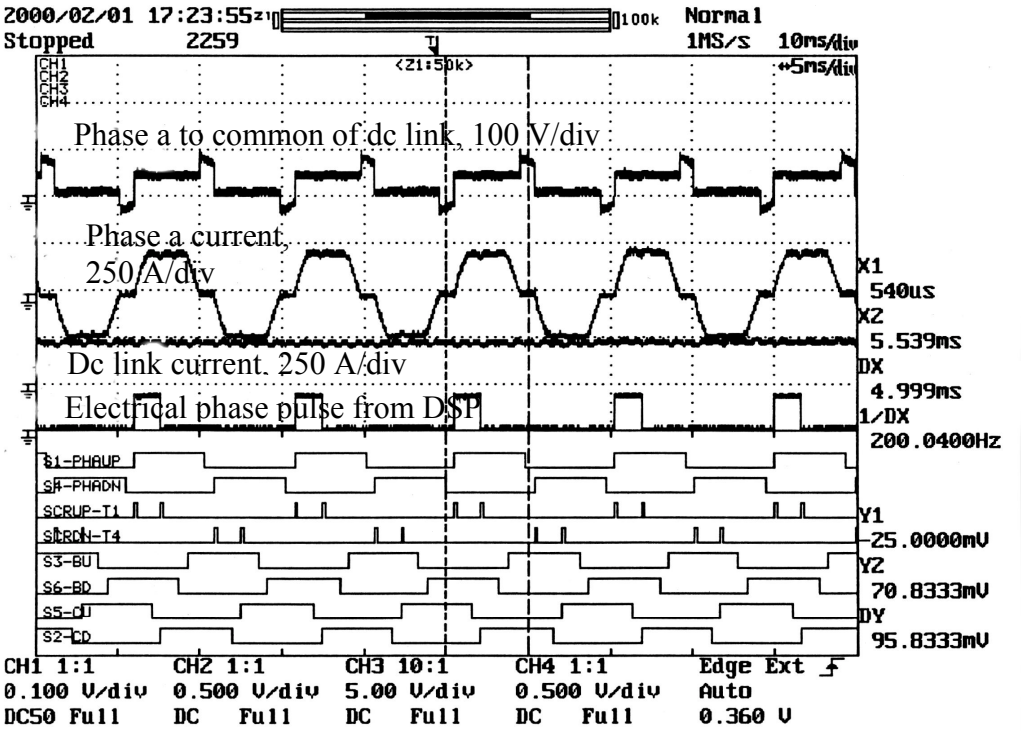

Fig. 3.3. Run 3.

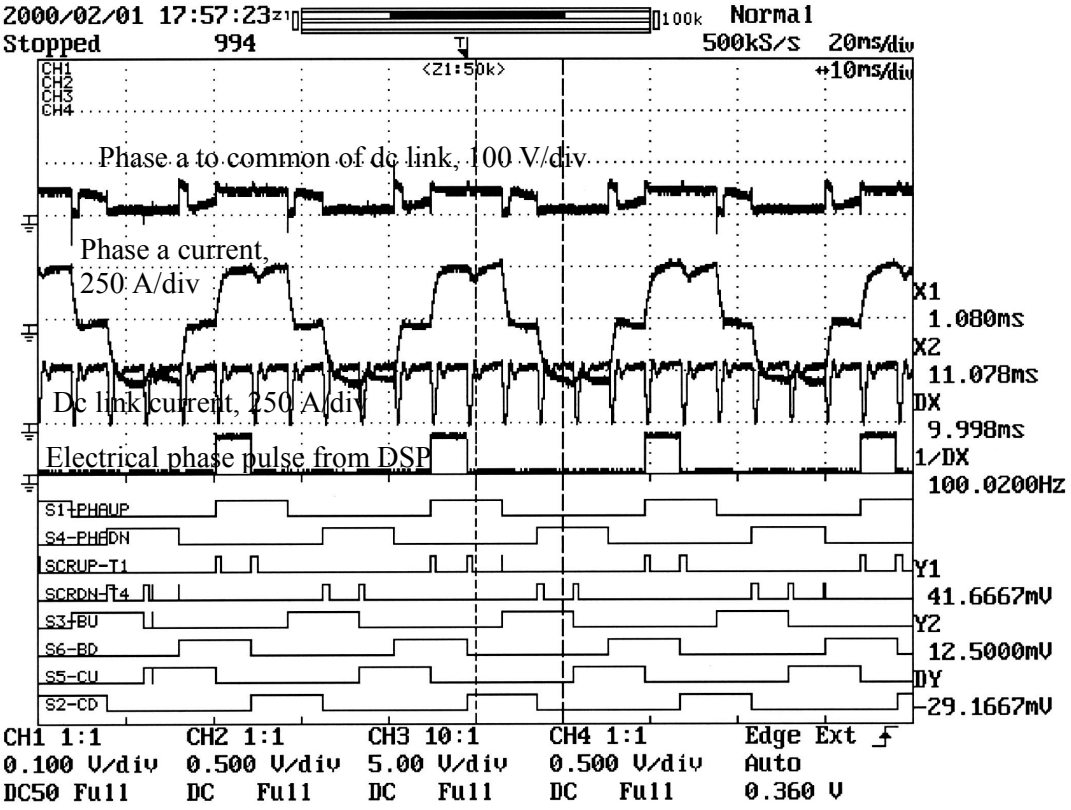

Fig. 3.4. Run 4.

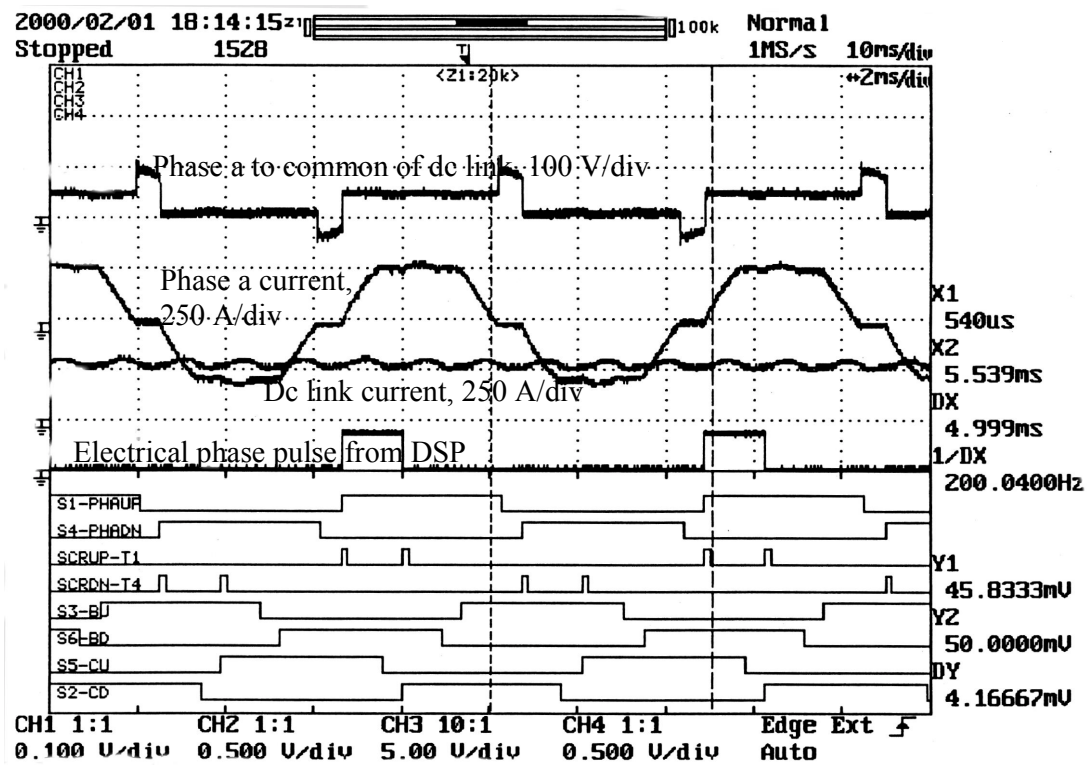

Fig. 3.5. Run 5.

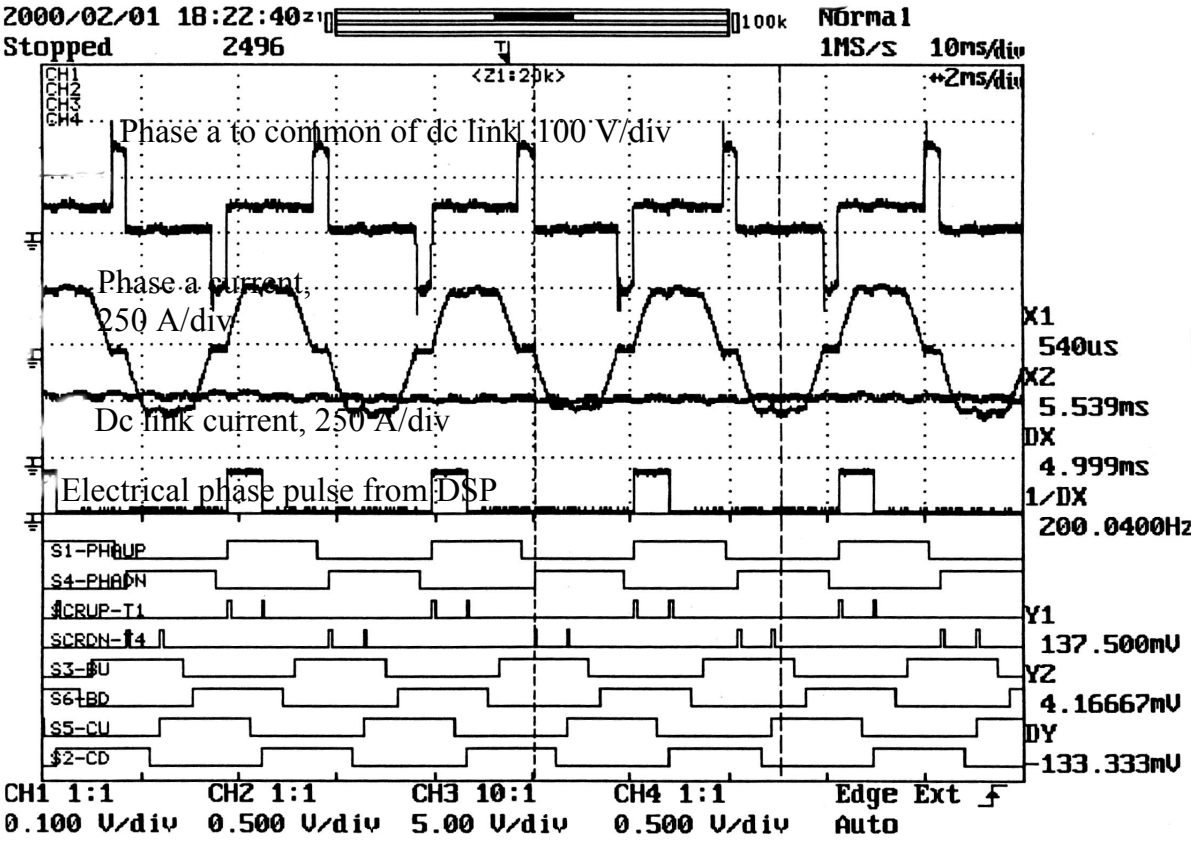

Fig. 6. Run 6.

3.3 Conclusions

Figure 3.7 shows that the DMIC could indeed produce the rated power while maintaining a relative constant current over the CPSR of six. Figure 3.8 indicates that the DMIC is somewhat insensitive to voltage variations as the speed is increased.

The next steps in the process of verifying the DMIC are:

1) A 20 hp motor is being built that has a base speed of 700 rpm and a CPSR of 4.5.
2) An integrated DMIC with a speed control loop is being built to operate with the 20 hp motor.

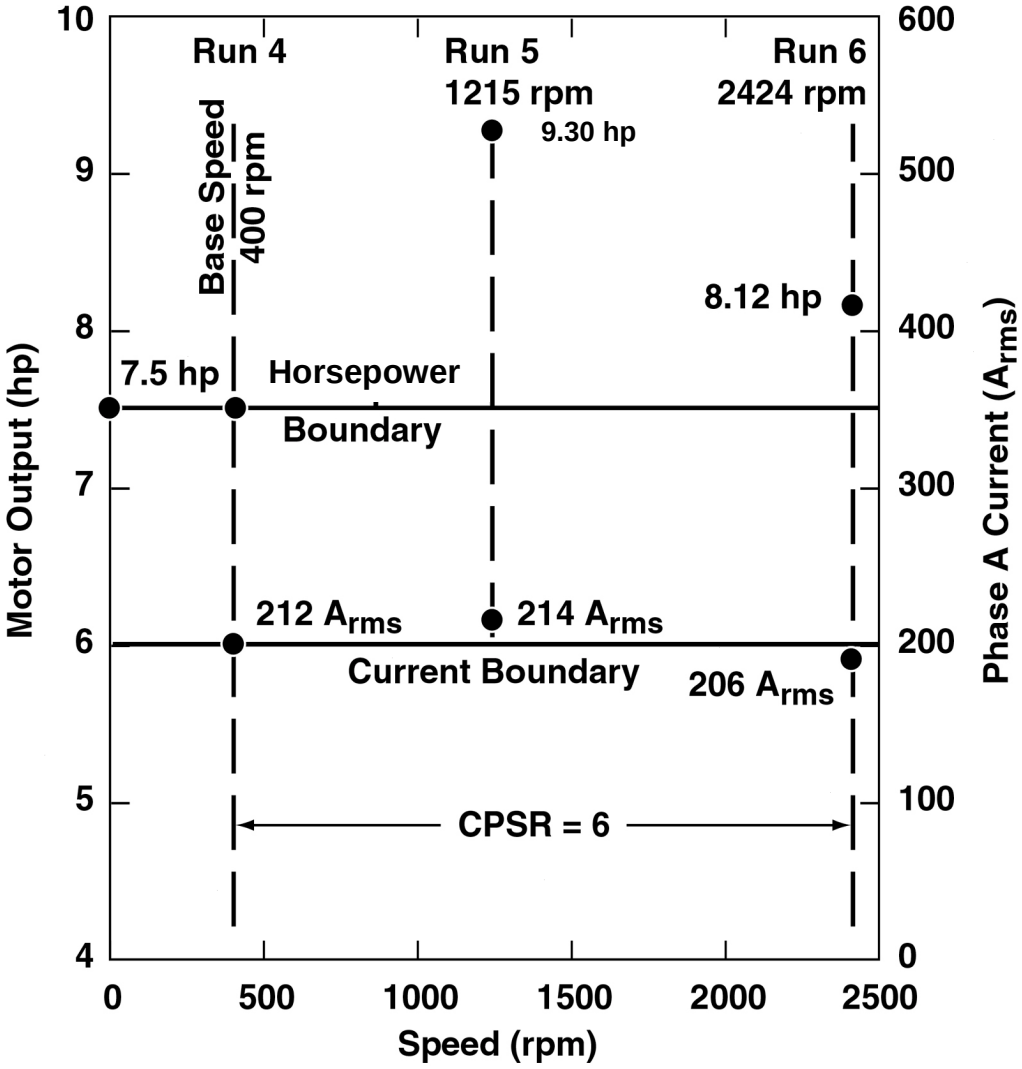

Fig. 3.7. Verification runs at 41.9V dc link supply.

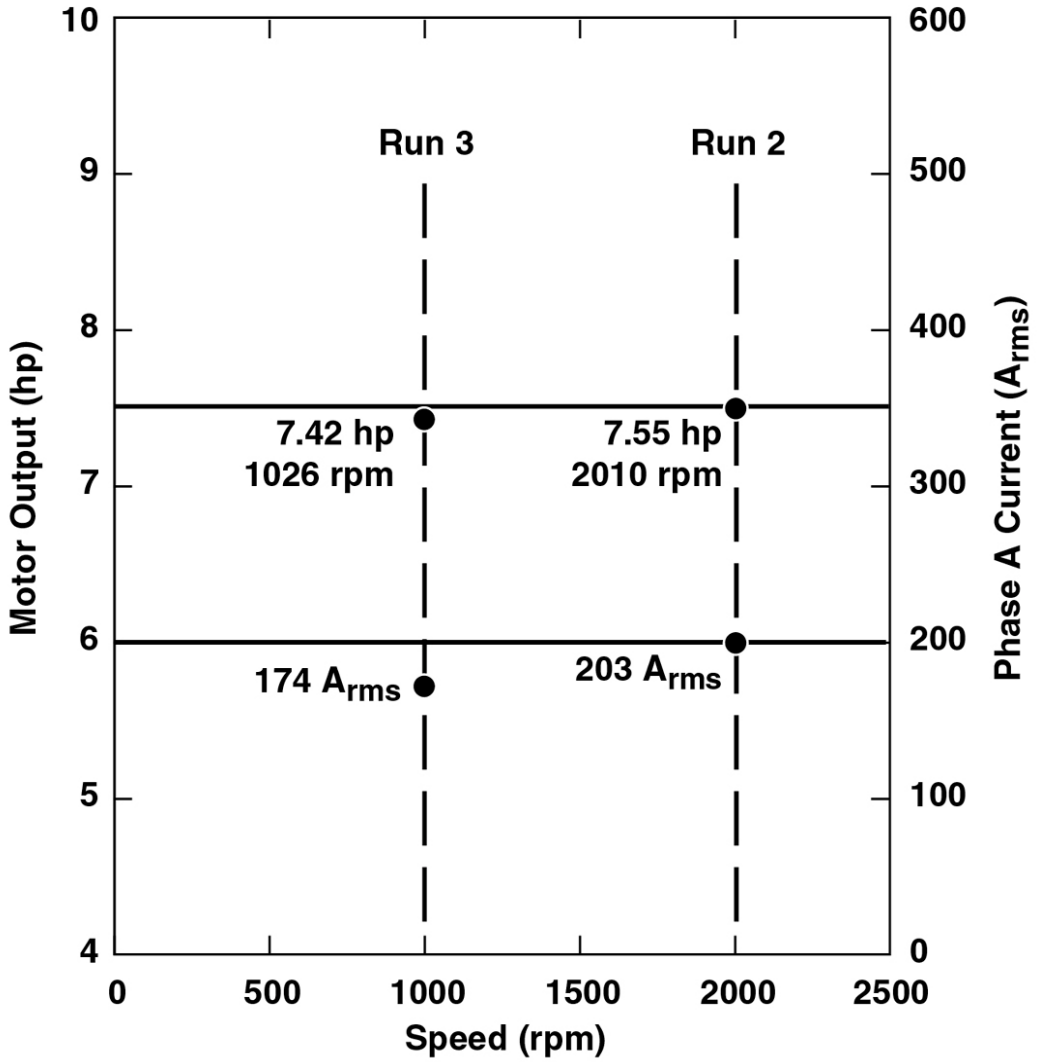

Fig. 3.8. Voltage sensitivity at 40V dc link supply.

4. REFERENCES

1. J. M. Bailey, J. S. Lawler, and H. W. Blake, *Field-Weakening Schemes and Magnet-Retention Techniques for Permanent Magnet Machines*, ORNL/TM-1999/74, Oak Ridge National Laboratory, Lockheed Martin Energy Research Corporation, 1999.

2. Cambier et al., *Brushless DC Motor Using Phase Timing Advancement*, U.S. Patent Number 5,677,605, October 14, 1997.

3. T. Sabastian and G. R. Slemon, "Operating Limits of Inverter-Driven Permanent Magnet Motor Drives," pp. 327–333 in *IEEE Transactions*, **IA-23,** 1987.

4. J. S. Lawler, J. M. Bailey, and J. W. McKeever, *Extended Constant Power Speed Range of the Brushless DC Motor through Dual Mode Inverter Control,* ORNL/TM-2000/130, Oak Ridge National Laboratory, UT-Battelle, LLC, 2000.

5. Yokogawa Electric Corporation, *PZ4000 Power Analyses User Manual*, IM253710-OIE, First Edition, App. 4.

APPENDIX A

WATER BRAKE DETAILS

KAHN SERIES 101 GENERAL PURPOSE DYNAMOMETERS

FOR LOAD TESTING OF SMALL GAS TURBINES, GASOLINE ENGINES, AUXILIARY POWER UNITS, ELECTRIC AND HYDRAULIC MOTORS, HIGH SPEED GEARBOXES, BELT AND CHAIN DRIVES.

FEATURES

- Easy to install and to operate
- Lightweight, portable units with standard AND 10266/10262 mounting flange
- Hardened stainless steel power elements providing superior resistance to cavitation and corrosion
- Straightforward design permitting quick overhaul
- Spring loaded, precision ball bearings—grease packed or oil mist lubricated
- Water cooled quality carbon face seal
- Built-in 60 tooth gear for use with magnetic speed pickup
- Full power absorption in either direction of rotation

OPERATING PRINCIPLE

A single perforated disc rotates in a housing between perforated stators. Cold water enters the rotor chamber at the center. The water is accelerated by the rotating disc and thrown outwards. From the outer diameter of the rotor chamber inwards, the water forms an annulus which rotates at approximately half of the angular disc speed. The centrifugal pressure resulting from this process, forces the hot water out of the rotor chambers.

Power is absorbed—and converted into heat—by water vortices generated in rotor and stator holes. The resulting drag applies a resistance to rotation and tends, with an equal effort, to turn the dynamometer housing in the trunnion bearings. The housing is restrained from turning by a load cell which is mounted to the torque arm at a fixed distance from the centerline of the dynamometer.

The amount of power absorbed by the dynamometer is a function of water level (size of rotating water annulus) and speed. The water level is modulated with the inlet and outlet control valves. At a given speed, maximum power is absorbed when the rotor chambers are completely filled with water.

WATER SUPPLY REQUIREMENTS

Hydraulic dynamometers convert mechanical energy into heat. The heat is dissipated by a continuous flow of water through the dynamometer. The flow rate is proportional to the amount of power absorbed.

Water Flow*	4 gal/hr hp (20 l/hr kW)
Supply Pressure	50 psig (3.5 bar)
Max. Inlet Temperature	90°F (32C)
Max. Outlet Temperature	180°F (82°C)
Filtration	20 mesh screen
Seal Water Flow	0.1 gal/min (0.4 l/min)

*at delta t – 76°F (42°C)

ROTOR ASSEMBLY

Single perforated disc mounted on shaft by means of an involute spline. Shaft and disc made from hardened stainless steel. 60-tooth shaft mounted gear. Entire rotor assembly dynamically balanced.

BEARINGS, LUBRICATION AND SEAL

Two ABEC 5 or ABEC 7 precision ball bearings. Spring loaded to reduce vibration. Grease packed or oil mist lubricated. Oil mist lubricated units with one removable oil injector per bearing. Including wall mounted oil mist system with air pressure regulator, filter and lubricator.

Lubricating Oil	MIL-L-7808 or Mobil DTE 24
Oil Reservoir Capacity	19 oz. (.56 l)
Air Requirements	max. 5.0 scfm dry air
Air Supply Pressure	50-100 psig (3.5-7.0 bar)

Stationary carbon face seal with chrome plated mating ring. Continuously cooled with water to prevent distortion and cracking of the carbon ring. Any water leakage across the carbon face seal is discharged by a rotating flinger into a drain cavity.

HOUSING AND TRUNNION MOUNT

Lightweight aluminum housing supported by two grease packed trunnion bearings. Trunnion mount with AND 10266/10262 mounting flange. Rotor chamber lined with hardened stainless steel stator plates. Built-in vacuum breaker to maintain atmospheric pressure in the rotor chamber.

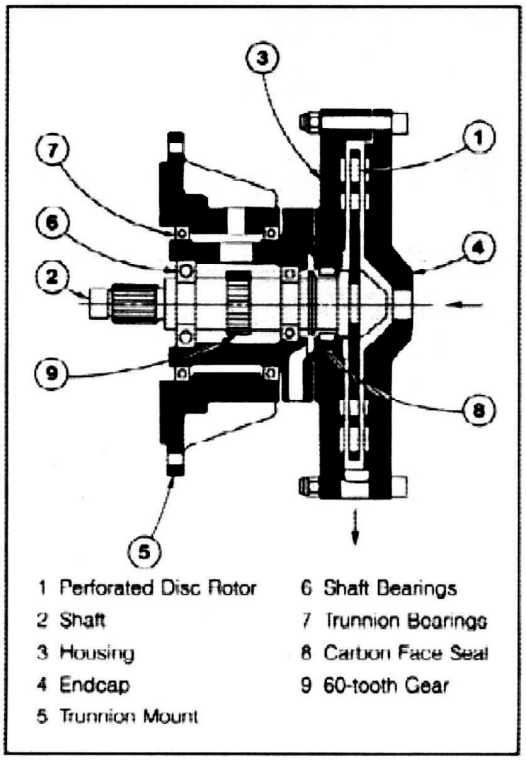

1 Perforated Disc Rotor
2 Shaft
3 Housing
4 Endcap
5 Trunnion Mount
6 Shaft Bearings
7 Trunnion Bearings
8 Carbon Face Seal
9 60-tooth Gear

Fig. A.1. Kahn Series 101 Dynamometer.

SPECIFICATIONS

Model	Max. Power hp	Max. Speed rpm	Max. Torque ft.lb.	WR² in²lb	Dry Weight lbs
101-080	450	11,500	250	21	50
101-100	700	11,500	450	57	60
101-130	1000	9,000	600	180	85

OPERATING RANGE

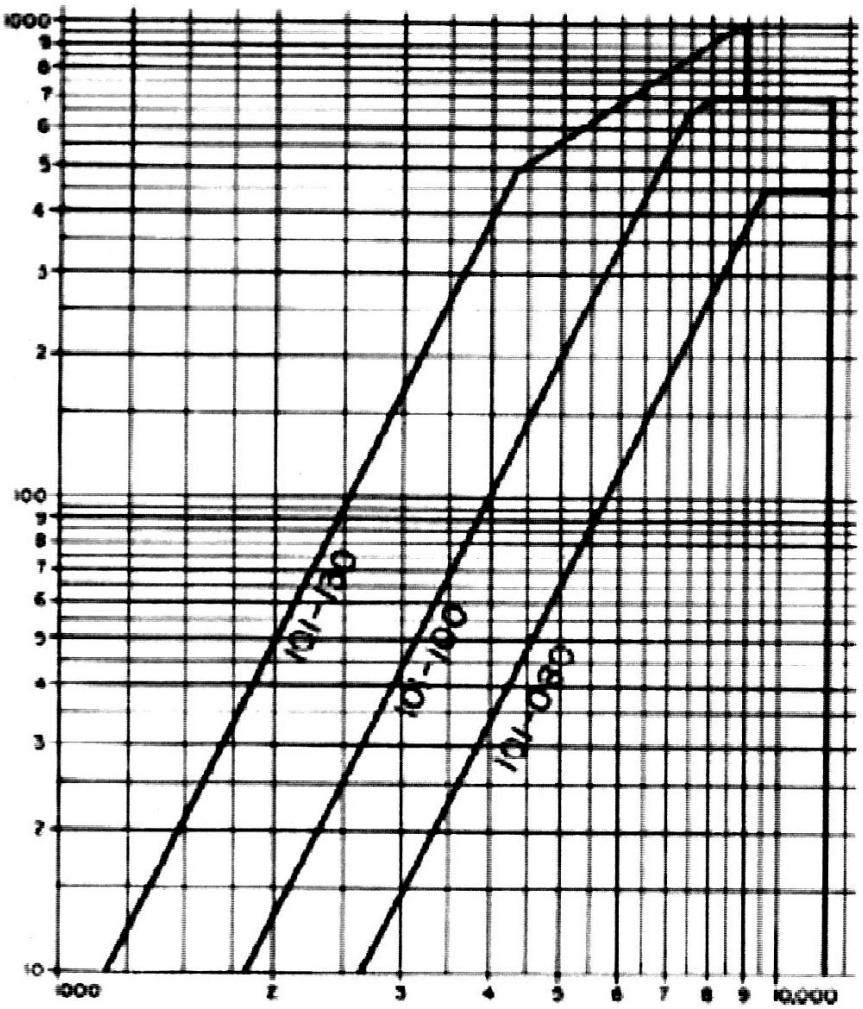

Fig. A.2. Horsepower absorbed vs rpm speed.

APPENDIX B

FILE NAMES AND TIME/DIVISION

DISK 1
PZ400 POWER METER

RUN NO.	FILE NAME	INFORMATION	FILE TYPE
1	FWPZ 000 001 002 003 004 005	V_{AC} I_A V_{BC} I_B V_{LINK} (dc) I_{LINK} (dc)	III. TIFF TIFF TIFF TIFF TIFF TIFF
2	006 007 008 009 010 011 012	V_{AC} I_A V_{BC} I_B V_{LINK} (dc) I_{LINK} (dc) Full Numeric Data	IV. TIFF TIFF TIFF TIFF TIFF TIFF TIFF

DISK 2
PZ4000 POWER METER

RUN NO.	FILE NAME	INFORMATION	FILE TYPE
2	FWPZ 000 001 002 003	V_{AC} I_A V_{BC} I_B	V. ASC11 ASC11 ASC11 ASC11

DISK 3
PZ4000 POWER METER

RUN NO.	FILE NAME	INFORMATION	FILE TYPE
2	FWPZ 000 CVS 001 CVS	V_{Link}(dc) I_{Link}(dc)	VI. ASC11 ASC11

DISK 4
YOKOGAWA PZ4000 POWER METER

RUN NO.	FILE NAME	VARIABLE	FILE TYPE
4	FWPZ 000 001 002	I_A I_{link}(dc) Full Numeric Data	VII. TIFF TIFF TIFF
5	FWPZ 003 004	I_A I_{LINK}(dc)	VIII. TIFF TIFF
6	FWPZ 005 006 007 008	Full Numberic Data I_A V_{AC} I_{LINK}(dc)	IX. TIFF TIFF TIFF TIFF

DISK 5
YOKOGAWA PZ4000 POWER METER

RUN NO.	FILE NAME	VARIABLE	FILE TYPE
6	FWPZ 000 CSV 001 CSV 002 CSV 003 CSV 004 CSV 005 CSV	I_{link}(dc) I_A V_{AC} V_{BC} I_B V_{Link} (dc)	X. ASC11 ASC11 ASC11 ASC11 ASC11 ASC11

DISK 6
YOKOGAWA DL7100 OSCILLOSCOPE

RUN NO.	FILE NAME	VARIABLE
1 2 4	FWDL 000 FWDL 001 FWDL 002	Full Screen Full Screen Full Screen

DISK 7
TEKTRONIC OSCILLOSCOPE

RUN NO.	FILE NAME	VARIABLE	FILE TYPE
3	TEKO	Two Hall Probes and I_A	TIFF
4	001	Two Hall Probes and I_A	TIFF

Most oscilloscopes give direct time/division readings. The Yokogawa DL7100 oscilloscope gives the time/division and, if zoomed to spread the data out, also gives the time/division at the zoomed rate. These numbers are visible on the screen and on tiff outputs. The PZ4000 power meter doesn't have that kind of output on its waveform screen. The time/division can be calculated with the data that is on the screen of a tiff file. The time/division for the PZ4000 waveforms are given below

	Disk #	Run #	Filename	Time/Division
	1	1	FWPZ000.TIF	1 ms/division
	1	1	FWPZ001.TIF	1 ms/div
	1	1	FWPZ002.TIF	1 ms/div
	1	1	FWPZ003.TIF	1 ms/div
	1	1	FWPZ004.TIF	1 ms/div
	1	1	FWPZ005.TIF	1 ms/div
	1	2	FWPZ006.TIF	1 ms/div
	1	2	FWPZ007.TIF	1 ms/div
	1	2	FWPZ008.TIF	1 ms/div
	1	2	FWPZ009.TIF	1 ms/div
	1	2	FWPZ010.TIF	1 ms/div
	1	2	FWPZ011.TIF	1 ms/div
	1	2	FWPZ012.TIF	1 ms/div
	4	4	FWPZ000.TIF	10 ms/div
	4	4	FWPZ001.TIF	1 ms/div
	4	4	FWPZ002.TIF	numeric data
	4	5	FWPZ003.TIF	4 ms/div
	4	5	FWPZ004.TIF	4 ms/div
	4	5	FWPZ005.TIF	numeric data
	4	6	FWPZ006.TIF	1 ms/div
	4	6	FWPZ007.TIF	1 ms/div
	4	6	FWPZ008.TIF	1 ms/div

As a check, one can look at the oscilloscope output for the run number of the tiff file being viewed, then compare to the power meter output for accuracy. For instance, run #4's oscilloscope tiff files havethe direct time/division on them, and can be compared to all of run #4's power meter tiff files to make sure the time/division is correct.

DISTRIBUTION

1. D. J. Adams
2. C. W. Ayers
3. J. M. Bailey
4. C. L. Coomer
5. E. C. Fox
6. D. B. Hamilton, DOE/OAAT, 1000 Independence Avenue, FORS, EE-32, Rm. 5G-023, Washington, D.C. 20585
7. J. S. Hsu
8. R. S. Kirk, DOE/OAAT, 1000 Independence Avenue, FORS, EE-32, Rm. 5G-046, Washington, D.C. 20585
9. R. A. Kost, DOE/OAAT, 1000 Independence Avenue, FORS, EE-32, Rm. 5G-045, Washington, D.C. 20585
10. J. S. Lawler, The University of Tennessee–Knoxville, Department of Electrical & Computer Engineering, Knoxville, Tennessee 37996-2100

11–40. J. W. McKeever

41. J. A. Merritt, DOE/OAAT, 1000 Independence Avenue, FORS, EE-32, Rm. 5G-064, Washington, D.C. 20585
42. G. W. Ott, Jr.
43. P. Overholt, DOE/OPWT, 1000 Independence Avenue, FORS, EE-11, Rm. 5H-065, Washington, D.C. 20585
44. R. M. Schilling
45. M. B. Scudiere
46. G. J. Su
47. R. A. Sutula, DOE/OAAT, 1000 Independence Avenue, FORS, EE-32, Rm. 5G-046, Washington, D.C. 20585
48. W. Van Dyke, DOE-HQ, Office of Disposition Technologies, 19901 Germantown Road, GTN, Rm. B-433, NE-40, Germantown, Maryland 20874-1290
49. C. P. White
50. R. E. Ziegler

51-52. Laboratory Records for submission to OSTI (2)